The Global Symplectic Integrator: an efficient tool for stability studies of dynamical systems. Application to the Kozai resonance in the restricted three-body problem

Libert, Anne-Sophie; Hubaux, Charles; Carletti, Timoteo

Published in:
Monthly Notices of the Royal Astronomy Society

Publication date:
2011

Document Version
Early version, also known as pre-print

Symplectic integration of deviation vectors and chaos determination. Application to the Hénon-Heiles model and to the restricted three-body problem.

A.-S. Libert, Ch. Hubaux and T. Carletti

Department of Mathematics FUNDP, 8 Rempart de la Vierge, B-5000 Namur, Belgium

E-mail: anne-sophie.libert@fundp.ac.be, charles.hubaux@fundp.ac.be, timoteo.carletti@fundp.ac.be

Abstract. In this work we propose a new numerical approach to distinguish between regular and chaotic orbits in Hamiltonian systems, based on the simultaneous integration of both the orbit and the deviation vectors using a symplectic scheme, hereby called *global symplectic integrator*. In particular, the proposed method allows us to recover the correct orbits character with very large integration time steps, small energy losses and short CPU times. To illustrate the numerical performances of the global symplectic integrator we will apply it to two well-known and widely studied problems: the Hénon-Heiles model and the restricted three-body problem.

PACS numbers: 05.45.-a, 45.10.-b, 05.45.Pq

1. Introduction

Hamiltonian systems exhibit phase spaces where regular and chaotic orbits do coexist. This fact makes the problem of the numerical characterization of regular and chaotic motion an hard task, notably in systems with many degrees of freedom. For this reason scientists developed fast and accurate tools to obtain information about the chaotic versus regular nature of the orbits of such systems, and efficiently characterize large domains in their phase space as ordered or (weakly) chaotic.

These methods can be roughly divided into two major groups: *Lyapunov–like* methods, i.e. methods based on the study of the evolution of deviation vectors for a given orbit; the methods FLI [1], `MEGNO` [2], `SALI` [3] and `GALI` [4] belong to this first class. And *Fourier–like* methods based on the determination of the frequencies of the spectrum of some observable related to a given orbit, for instance `FMA` [5, 6] or the Spectral method [7]. In the present work we will be interested in the former class, in particular to the `SALI` chaos detection technique.

To numerically compute such an indicator, one needs to have a good orbit determination, but also to integrate the evolution of two deviation vectors. It is well-known that symplectic integration schemes outperform the non–symplectic ones, when compared using the same order of accuracy and the same integration step size. This is mainly due to the very good energy conservation properties, but also to other first integrals. As a consequence, larger step sizes are allowed while still keeping a reasonably small energy loss. Thus they allow us to enlarge considerably the time span of the numerical simulation, without degradating the goodness of the numerical results, that is why symplectic integrators turn out to be essential for the long-term evolution of a dynamical system.

In the same way, chaos detection techniques could also benefit from the use of symplectic integrators. The aim of this paper is to show that the symplectic integration of the deviation vectors can improve the ability of the previous chaos indicators in the characterization of regular and chaotic orbits by correctly identifying the orbit behavior, using a larger integration step size. Because our method propose to integrate simultaneously both the orbit and the deviation vectors, using a symplectic scheme, we hereby name this method *global symplectic integrator*.

More precisely, we will accurately determine, using a symplectic scheme and a small enough integration time step τ, the character, i.e. the regular or chaotic behavior, of a large number, N_{tot}, of orbits using one of the aforementioned chaos detectors. Then, all the previous orbits will be reanalyzed using both symplectic and non-symplectic integrators schemes, but with larger and larger time steps. We will show that the use of the global symplectic integrator will allow us to recover a large percentage of orbits' characters with very large time steps compared to the non–symplectic one and using small amount of CPU time.

Our symplectic method will be applied to the classical Hénon–Heiles model, and also to a well-known problem of celestial mechanics: the restricted three-body problem,

where the possibility of using large integration step sizes is essential for the study of secular resonances.

The paper is organized as follows. In Section 2, we describe our method for integrating symplectically the deviation vectors used in the chaos detection techniques. For the sake of completeness, we present, in Section 3, a brief introduction to the `SALI` chaos indicator. The results of our method applied to the Hénon–Heiles system are presented in Section 4.1, while Section 4.2 will be devoted to present an application to the restricted three-body problem. Finally in Section 5 we will summarize our findings and we will conclude.

2. The method

Let us consider a generic Hamiltonian vector field

$$\dot{\vec{x}} = J\nabla_x H(\vec{x})\,, \tag{1}$$

where $\vec{x} = (\vec{p}, \vec{q}) \in R^{2n}$ is the momentum–position vector in the phase space, $H(\vec{x})$ is the Hamilton function describing the system and $J = \begin{pmatrix} 0_n & -1_n \\ 1_n & 0_n \end{pmatrix}$ is the standard constant symplectic matrix. The solution of (1) with initial datum $\vec{x}_0$ can be formally written as

$$\varphi(t) = e^{tL_H}\vec{x}_0\,, \tag{2}$$

where L_H is the Lie operator, i.e. for all smooth function defined in the phase space we have $L_H f = \{H, f\}$, being $\{\cdot,\cdot\}$ the Poisson bracket.

Given a deviation vector $\vec{v}$, its time evolution is described by the *tangent map*:

$$\frac{d\vec{v}}{dt} = M\left(\varphi(t)\right)\vec{v}\,, \tag{3}$$

where M is the Jacobian of the Hamiltonian vector field (1), namely $M = J\nabla_x^2 H$, evaluated on the solution $\varphi(t)$.

Because $\nabla_x^2 H$ is a symmetric matrix, the matrix M is an Hamiltonian one, i.e. $M^T J + JM = 0$. Hence also the vector field (3) is Hamiltonian, with Hamiltonian function

$$K(\vec{v}) = \frac{1}{2}\vec{v}^T S\vec{v}\,, \tag{4}$$

where $S = \nabla_x^2 H$.

Let us now assume that the function H can be decomposed into the sum of two parts each one separately integrable, for instance each one depending only on one group of variables

$$H(\vec{x}) = A(\vec{p}) + B(\vec{q})\,. \tag{5}$$

Let us observe that in the case of the restricted three-body problem (see Section 4.2), we will prefer to use a different splitting of the Hamiltonian function: actually the function A will correspond to two non-interacting two-body problems that in rectangular

coordinates will thus result a function of positions and momenta; while the remainder will be by definition the B function.

Under the above assumptions, a family of suitable symmetric symplectic schemes has been presented in [8], hereby called $SABA_n$. Such methods develop the solution given by (2) using the Baker–Campbell–Hausdorff formula [9], allowing to approximate the true solution by a finite number of compositions of integrable symplectic maps, being the error of the approximation a function of the integration step size τ.

More precisely one can find coefficients $(c_i)_{i=1,\dots,n+1}$ and $(d_i)_{i=1,\dots,n}$ such that the map

$$SABA_n(\vec{x}) = e^{c_1\tau L_A} e^{d_1\tau L_B} \dots e^{d_n\tau L_B} e^{c_{n+1}\tau L_A} e^{d_n\tau L_B} \dots e^{d_1\tau L_B} e^{c_1\tau L_A}(\vec{x}) \,, \quad (6)$$

is symmetric under the transformation $t \mapsto -t$, is symplectic and is of order $\mathcal{O}(\tau^{2n})$, namely there exists an Hamiltonian function $\tilde{H}$ whose exact flow is given by (6) and moreover $\tilde{H} = H + \mathcal{O}(\tau^{2n})$.

Rewriting the deviation vector as $\vec{v} = (\vec{v}_p, \vec{v}_q)$, i.e. identifying its components with the natural splitting of the phase space, we can explicitely write the Hamiltonian K as follows:

$$K(\vec{v}) = \frac{1}{2}\vec{v}_p^T \mathcal{A}(\vec{p})\vec{v}_p + \frac{1}{2}\vec{v}_q^T \mathcal{B}(\vec{q})\vec{v}_q \,, \quad (7)$$

where

$$\mathcal{A}(\vec{p}) = \nabla_p^2 A(\vec{p}) \quad and \quad \mathcal{B}(\vec{q}) = \nabla_q^2 B(\vec{q}) \,. \quad (8)$$

Hence the symmetric symplectic methods $SABA_n$ can be used also to integrate the evolution of the deviation vectors.

The aim of this paper is to show that the use of a symplectic integrator to solve both the orbit evolution and the tangent equation, i.e. to get the time evolution of the deviation vector, can improve the capability of some widely used chaos indicators (such as `SALI`) to determine the character of the orbits in an Hamiltonian system.

Our claim will be numerically proved for the Hénon–Heiles system, using $SABA_4$ and $SABA_2$ symplectic schemes in comparison with the non–symplectic 4^{th} order Runge–Kutta method (see Section 4.1); while $SABA_{10}$ and Bulirsch-Stoer will be used for the study of the restricted three-body problem (see Section 4.2). In the rest of the paper the easily implementable `SALI` chaos detection technique will be used to numerically determine the orbit character. For the sake of completeness, the next section will be devoted to a brief introduction of the above mentioned chaos indicator.

3. The SALI chaos indicator

The Smaller ALignment Index, `SALI` [3], has been proved to be an efficient and simple method to determine the regular or chaotic nature of orbits in conservative dynamical systems. Thanks to its properties it has been already successfully applied to distinguish between regular and chaotic motion both in symplectic maps and Hamiltonian flows (e.g. [10, 11, 12, 13]).

For the sake of completeness let us briefly recall the definition of the SALI and its behavior for regular and chaotic orbits, restricting our attention to symplectic flows. The interested reader can consult [3, 14] to have a more detailed description of the method. To compute the SALI of a given orbit, one has to follow the time evolution of the orbit itself and also of two linearly independent unitary deviation vectors $\hat{v}_1(0), \hat{v}_2(0)$. The evolution of an orbit is given by (2), while the evolution of each deviation vector is given by the tangent map (3).

Then, according to [3] the SALI for the given orbit is defined by

$$\mathtt{SALI}(t) = \min\left\{\|\hat{v}_1(t) + \hat{v}_2(t)\|, \|\hat{v}_1(t) - \hat{v}_2(t)\|\right\}, \tag{9}$$

where $\|\cdot\|$ denotes the usual Euclidean norm and $\hat{v}_i(t) = \frac{\vec{v}_i(t)}{\|\vec{v}_i(t)\|}$, $i = 1, 2$, are normalized vectors.

In the case of chaotic orbits, the deviation vectors $\hat{v}_1$, $\hat{v}_2$ eventually become aligned in the direction defined by the maximal Lyapunov characteristic exponent [15] (LCE), and $\mathtt{SALI}(t)$ falls exponentially to zero. An analytical study of SALI's behavior for chaotic orbits was carried out in [14] where it was shown that

$$\mathtt{SALI}(t) \propto e^{-(\sigma_1 - \sigma_2)t}, \tag{10}$$

with σ_1, σ_2 being the two largest LCEs.

In the case of regular motion, on the other hand, the orbit lays on a torus and the vectors $\hat{v}_1$, $\hat{v}_2$ eventually fall on its tangent space, following a t^{-1} time evolution, having in general different directions. In this case, the SALI oscillates about non zero values (for more details see [10]). This behavior is due to the fact that for regular orbits the norm of a deviation vector increases linearly in time. Thus, the normalization procedure brings about a decrease of the magnitude of the coordinates perpendicular to the torus at a rate proportional to t^{-1} and so $\hat{v}_1$, $\hat{v}_2$ eventually fall on the tangent space of the torus.

The simplicity of SALI's definition, its completely different behavior for regular and chaotic orbits and its rapid convergence to zero in the case of chaotic motion are the main advantages that make SALI an ideal chaos detection tool. Recently a generalization of the SALI, the so-called Generalized Alignment Index, GALI, has been introduced [4, 16], which uses information of more than two deviation vectors from the reference orbit. Since the advantages of GALI over SALI become relevant in the case of multi-dimensional systems, for the aim of the present paper we will restrict our attention to the SALI.

The scheme we used to numerically compute the SALI consists in integrating both the orbit and the deviation vector using the symmetric symplectic $SABA$ method and then compute the indicator according to the definition (9).

4. Results

In this section, we will present the results of the application of the global symplectic integrator to study the orbit behavior of two well-known problems: the Hénon–Heiles system and the restricted three-body problem. The analysis of the former widely studied

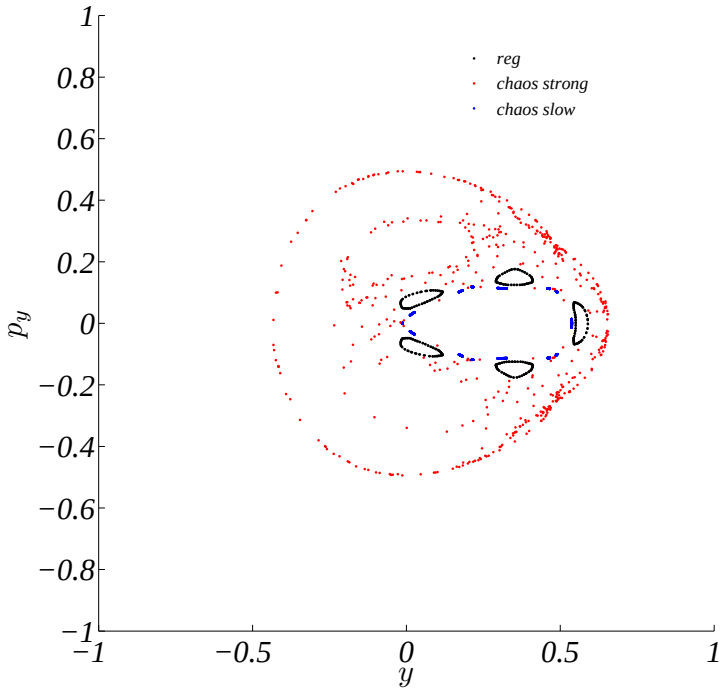

Figure 1. Hénon–Heiles phase space (section $x = 0$). The energy has been fixed to $E = 1/8$ and three characteristic orbits have been computed on this energy level: a regular orbit (black) with initial data $x(0) = 0$, $y(0) = 0.55$, $p_x \sim 0.2417$ and $p_y = 0$, a chaotic orbit strongly diffusing (red) with initial data $x(0) = 0$, $y(0) = -0.016$, $p_x \sim 0.49974$ and $p_y = 0$, and a chaotic orbit slowly diffusing (blue) with initial data $x(0) = 0$, $y(0) = -0.01344$, $p_x \sim 0.49982$ and $p_y = 0$.

dynamical system, will point out that chaos indicator can benefit from our method, regarding the characterization of regular and chaotic motion (see Section 4.1). The second application of our method consists in a classical problem of celestial mechanics, namely the restricted three-body problem, that will be presented in Section 4.2.

4.1. Hénon–Heiles system

The Hénon–Heiles Hamiltonian system [17] is a well-known and studied model described by the following Hamilton function

$$H(p_x, p_y, x, y) = \frac{1}{2}\left(p_x^2 + p_y^2 + x^2 + y^2\right) + x^2 y - \frac{1}{3}y^3 \,. \tag{11}$$

In the phase space, regular and chaotic orbits coexist (see Figure 1), whose character can be accurately and rapidly determined using `SALI` and integrating both the orbit and the deviation vectors using the $SABA_4$ scheme with a time step size $\tau = 10^{-4}$. The choice of a 4^{th} order integrator is motivated by a balance between reliability and computation time. Indeed, the smaller the used time step or the higher the integrator order, the better the energy preservation, but the longer the computation time. In this

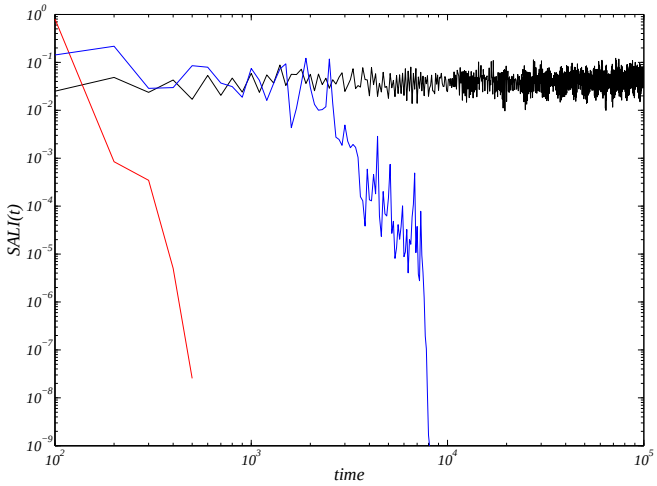

Figure 2. Characterization of the three orbits of Figure 1: a regular orbit (black), a chaotic orbit strongly diffusing (red) and a chaotic orbit slowly diffusing (blue). The integration step size has been fixed to $\tau = 10^{-4}$ and both the orbit and the deviation vectors have been numerically integrated using the $SABA_4$ method.

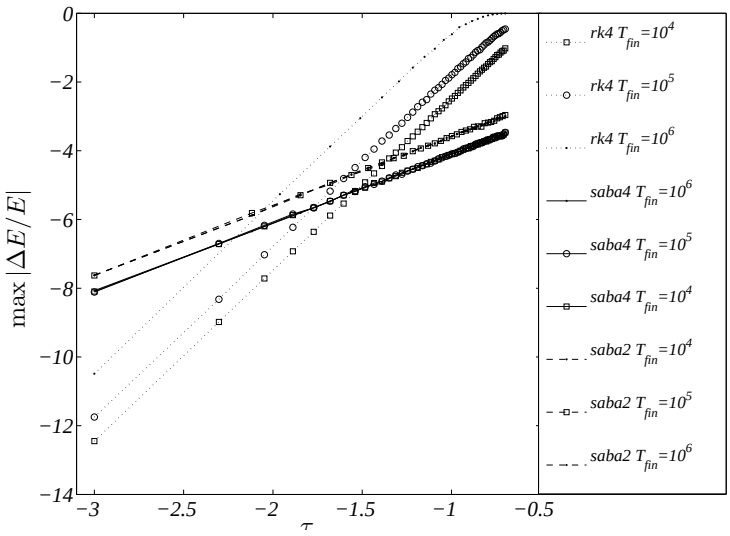

Figure 3. Relative energy loss, $\max_{0\leq t\leq T_{fin}} |\Delta E(t)/E(t)|$, for $SABA_4$, $SABA_2$ and $RK4$ integrators as a function of the time steps. Both quantities are given in logarithmic scale. Several integration times are selected, $T_{fin} = \{10^4, 10^5, 10^6\}$, as reported in the legend.

respect, we decided to adopt a $SABA_4$ integrator with a sufficiently small time step of $\tau = 10^{-4}$.

In Figure 2, we report the results of the numerical computation of the `SALI` for the three generic orbits of Figure 1. Since the characteristic period of the orbits on this energy level, is of the order of 10 time units, the integration time span has been

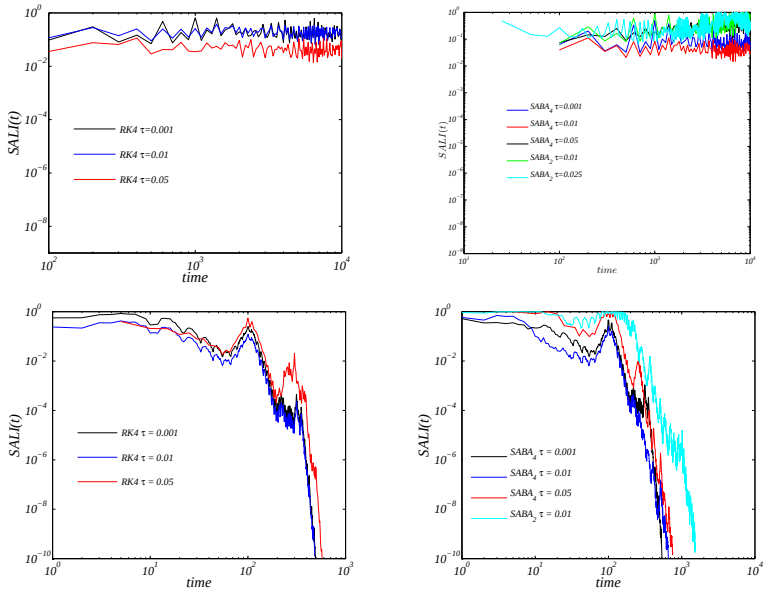

Figure 4. Comparison of integration schemes on the regular orbit $x = 0$, $y = 0.55$, $p_x \sim 0.2417$ (top panels) and $p_y = 0$ and on the chaotic orbit $x = 0$, $y = -0.016$, $p_x \sim 0.49974$ and $p_y = 0$ (bottom panels). Left panels, `SALI` computed using non-symplectic $RK4$ for time steps $\tau \in \{0.001, 0.01, 0.05\}$. Right panels, `SALI` computed using $SABA_4$ for the integration of both the orbit and the deviation vectors, for the same time steps. Both methods determine correctly the character of the orbits independently from the small time step used.

fixed to 10^4 time units. We can observe that the three possible dynamical behaviors, regular orbits, chaotic orbits strongly diffusing and chaotic orbits slowly diffusing, are well identified. Let us in fact observe that the strong chaotic behavior of the red orbit is translated to a quick decrease of `SALI` to zero. On the contrary, for the black regular orbit, `SALI` remains bounded away from zero. The blue orbit has a particular behavior: for quite a long time, up to $\sim 30\,000$ time units, this orbit "follows closely" a periodic, thus regular, orbit, and `SALI` remains positive, but eventually the chaotic character of the orbit manifests and the indicator correctly goes to zero. Actually the above orbit is close to an unstable periodic orbit.

To check the robustness of our method with respect to a non–symplectic one, we firstly reanalyze the above three orbits using larger time steps. More precisely, we numerically computed the `SALI` indicator using $SABA_2$, $SABA_4$ and $RK4$ integrators using time steps for which the energy loss is bounded by sufficient small value, 10^{-3}. This can be easily computed using the results of Figure 3, where we report the relative energy loss, averaged over 50 randomly chosen orbits, for the integrators $SABA_4$, $SABA_2$ and $RK4$, as a function of the time steps. For sake of completeness, we computed the relative energy loss using several integration time spans. Let us emphasize that, the energy losses for symplectic integrators are almost the same for all the integration time spans for a fixed value of τ, on the other hand the non–symplectic scheme $RK4$ exhibits

a strong dependence on the integration time span: the larger the time span is, the worst is the energy loss for a fixed value of τ. As expected, the larger the time step used, the larger the loss of energy. In the following, we fix the largest time steps, τ, such that the relative energy loss is smaller than 10^{-3}, for an integration time span equal to 10^4 time units. Under these assumptions we get: $\tau_{max} \sim 0.3$ for $SABA_4$, $\tau_{max} \sim 0.16$ for $SABA_2$ and $\tau_{max} \sim 0.08$ for $RK4$. As a result for the Hénon–Heiles system, our symplectic scheme allows time steps four times larger than a non-symplectic one of the same order, as will be shown hereafter.

With these maximal realistic time steps in mind, we reanalyzed the three orbits of Figure 2 with time steps $\tau \in \{10^{-3}, 0.01, 0.05\}$ for which the energy loss is small enough, even for the $RK4$ integrator. All the integration schemes behave almost equally for all the small used time steps, as it can observed from the results reported in Figure 4.

The next step of our comparison is to consider a larger portion of phase space to capture information on the characterization of the global dynamics using symplectic and non–symplectic integration schemes. We hence consider $N_{reg} = 100$ randomly chosen regular orbits and $N_{cha} = 100$ randomly chosen chaotic orbits, whose behavior has been accurately determined using a sufficiently small step size τ, namely $\tau = 10^{-4}$, and a 4^{th} order symplectic scheme. Then we compute as a function of the used step size, how many orbits are correctly characterized by the $RK4$ non-symplectic integration, and by the $SABA_2$ and $SABA_4$ symplectic integration for both the orbit and the deviation vectors.

On the one hand, the results reported in Figure 5 clearly show that, for regular orbits, almost all schemes are able to recover nearly 100% of regular orbits. Concerning the step sizes, Figure 5 shows that $SABA_4$ characterizes correctly the dynamics of the same percentage of orbits with 4 times larger time steps than $RK4$, while $SABA_2$ does the same with 2 times larger time steps than $RK4$, but observe that its order is half the one of $RK4$. On the other hand, the same conclusion holds for the chaotic orbits. Moreover, let us note a general trend of $RK4$ to overestimate the number of regular orbits when increasing the time step. Thus, our symplectic scheme is largely better than $RK4$ to characterize regular orbits, regarding both the used time step and the integration order. Indeed, $SABA_2$ symplectic integrations reveal to be nearly as reliable as $SABA_4$ ones, especially for small step sizes.

In Figure 6 we report the CPU times averaged over fifty randomly chosen orbits, T_{CPU}, as a function of the time steps. One can clearly observe that the symplectic schemes are faster than $RK4$ using the same step size, more precisely $SABA_4$ is almost 2.5 times faster than $RK4$. Once again this fact illustrates the good numerical performance of our method which is less time consuming in itself but also allows larger time steps, reducing again the computational time.

To quantify the *efficiency* of our symplectic scheme, we introduce the following efficiency indicator: $\varepsilon = p|\log_{10}(|\Delta E/E|)||\log_{10}(T_{CPU})|$, whose dependence as a function of the time step τ is represented in Figure 7. Let us observe that the larger is ε, the better is the integration scheme. For small integration time steps, the non-symplectic

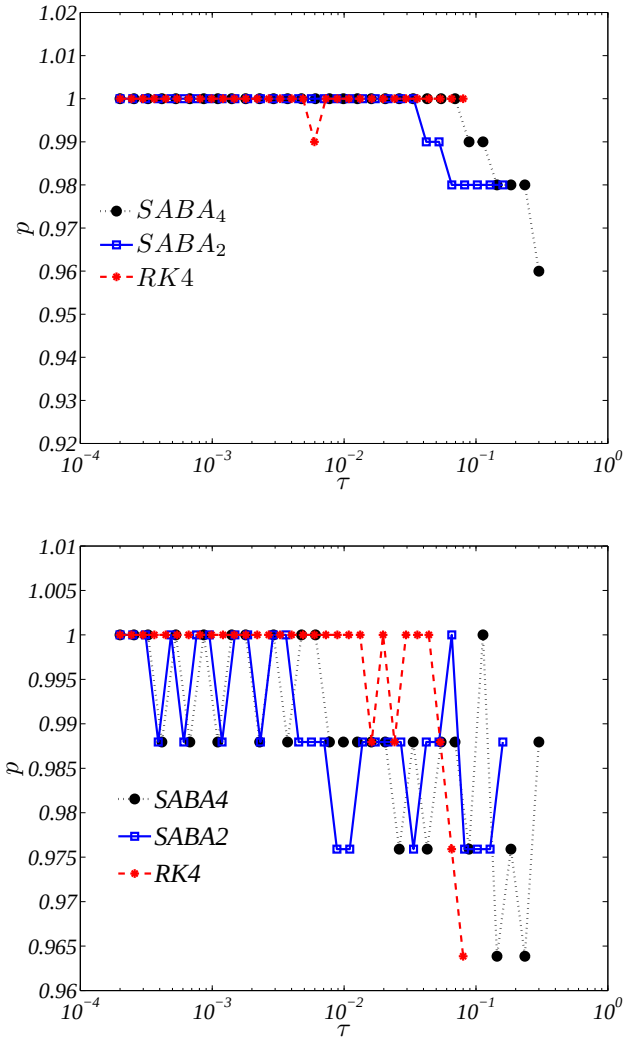

Figure 5. Global comparison between $RK4$ non–symplectic scheme and $SABA_4$, $SABA_2$ symplectic schemes for a large portion of the Hénon–Heiles phase space: $N_{reg} = 100$ regular orbits and $N_{cha} = 100$ chaotic orbits are considered. Top panel: Percentage of correctly identified regular orbits for increasing time steps (p = correctly identified orbits / total number of orbits). Bottom panel: Same as top panel for chaotic orbits.

$RK4$ scheme dominates, mainly because its energy loss is measly (see Figure 3). On the other hand, for time steps τ larger than 0.1, the situation is reversed: the global symplectic method dominates, as its energy loss and CPU times are both relatively small (see Figure 3 and 6), that results in a quite large efficiency.

As a result, it appears that the use of a symplectic integrator to compute the time evolution of the deviation vector can improve the capability of a chaos indicator such as `SALI` to determine the character of the orbits in a Hamiltonian system. Furthermore, we showed that our global symplectic integrator allows larger time steps without energy loss and saves a considerable amount of computation time. This possibility turns out to

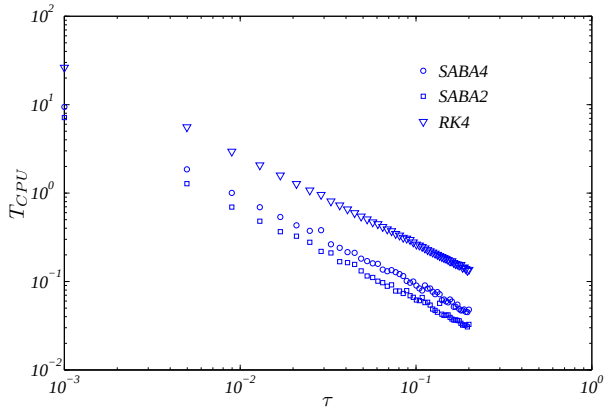

Figure 6. CPU time as a function of the time step τ. Both quantities are given in logarithmic scale. Linear best fits (data not shown) provide an almost linear decrease of T_{CPU} as a function of τ. The time integration span has been fixed to $T_{fin} = 10^4$.

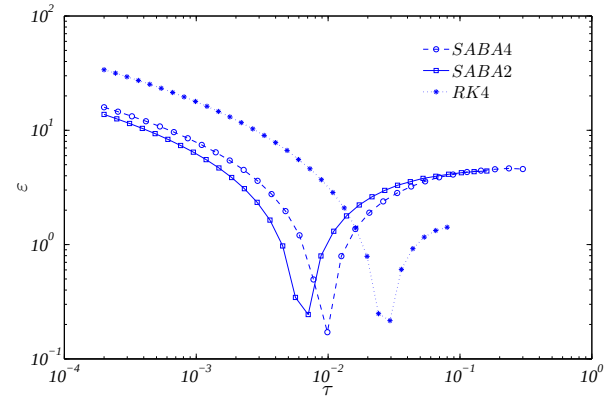

Figure 7. The efficiency $\varepsilon = p|\log_{10}(|\Delta E/E|)|\,|\log_{10}(T_{CPU})|$ of the global symplectic method ($SABA_4$ and $SABA_2$) and the non-symplectic one ($RK4$). The scales are logarithmic. See text for detail.

be essential for the study of real problems, where the time scales are fixed by physical constraints, as for instance in the case of secular resonances in the N-body celestial mechanics problem, as shown in the next section.

4.2. Restricted three-body problem

The problem of three celestial bodies interacting with each other gravitationally is a well-known problem in celestial mechanics. In the following we will consider the restricted problem. More precisely one of the bodies, hereby called the Sun, is the largest mass around which the two other bodies are assumed to evolve; the second body, possessing an intermediate mass hereby called Jupiter, orbits around the Sun on a circular orbit, while the third body, hereby called the asteroid, has a negligeable mass and is moving on an

inner orbit "between "the Sun and Jupiter. Assuming this geometry, Kozai [18] showed that a highly inclined asteroid perturbated by Jupiter is characterized by a coupled variation in its eccentricity e and inclination i, in such a way that $H = \sqrt{a(1-e^2)}\cos(i)$ is a constant, a being the asteroid's semi-major axis. This dynamics is often referred to as *Kozai resonance* (e.g. [19]).

Indeed, the restricted three-body problem can be reduced to two degrees of freedom after short-period averaging and node reduction (see for instance [20]). Assuming that the outer giant planet is on a circular orbit, this problem is integrable, and its dynamics can be represented on the phase space $(e\cos\omega, e\sin\omega)$ where ω is the argument of the pericentre of the massless body (see [21], [22] for more detail). Such a representation is given in Figure 8 where we plotted several trajectories of the small body obtained by the numerical integration of the Hamiltonian equations associated to the *democratic heliocentric* formulation (see for instance [23]) of the three-body problem:

$$K(P_i,Q_i) = \sum_{j=1}^{2}\left\{\frac{\|P_j\|^2}{2m_j} - G\frac{m_0 m_j}{\|Q_j\|}\right\} + \frac{1}{2m_0}\left\|\sum_{j=1}^{2} P_i\right\|^2 - G\sum_{j=1}^{2}\sum_{i=1}^{j-1}\frac{m_i mj}{\|Q_i - Q_j\|}\,. \quad (12)$$

To realize the representation of Figure 8, we used a 10^{th} order SABA integrator with a time step sufficiently small of $\tau = 10^{-3}$ years. This phase space corresponds to $H = 0.41833$, which means an inclination of 45° for the circular massless body represented on the center of the plot. As one can see, for that large inclination value, circular orbit corresponds to an unstable equilibrium point. A separatrix divides the phase space in three parts: two regions are characterized by the libration of ω respectively around 90° and 270° and a third one corresponding to a circulation of this angle. The two stable equilibria enclosed by the separatrix are referred to as Kozai equilibria. Hence, a massless body initially on a circular orbit will suffer from large variations in eccentricity, since its real motion (short periods included) will stay close to the separatrix of the reduced problem.

Let us note that these perturbations on a small body at high inclination are secular, which means that they operate on extremely long time scales (about $10,000$ years) compared to the annual orbital periodic variation of the bodies. Symplectic integrators are recommended for that kind of problem, as they possess good energy conservation properties and are efficient for large time steps. Our method for integrating symplectically the deviation vectors is then particularly suitable for the chaos determination of such a problem.

In Figure 9, we report the results of the numerical computation of the `SALI` with $SABA_{10}$ integrator ($\tau = 10^{-3}$ years) for a regular orbit ($e = 0.4$, i.e. close to one of the stable Kozai equilibria) and a chaotic orbit ($e = 0.001$, i.e. close to the unstable equilibrium). Our global symplectic integrator scheme reproduces correctly the expected character of both orbits in less than $40,000$ years.

Concerning the global behavior of the phase space, it can be thoroughly described by resorting to a chaos indicator technique along a cross section of the phase space. We choose to represent the `SALI` values as a function of the initial values for $e\sin\omega$, as

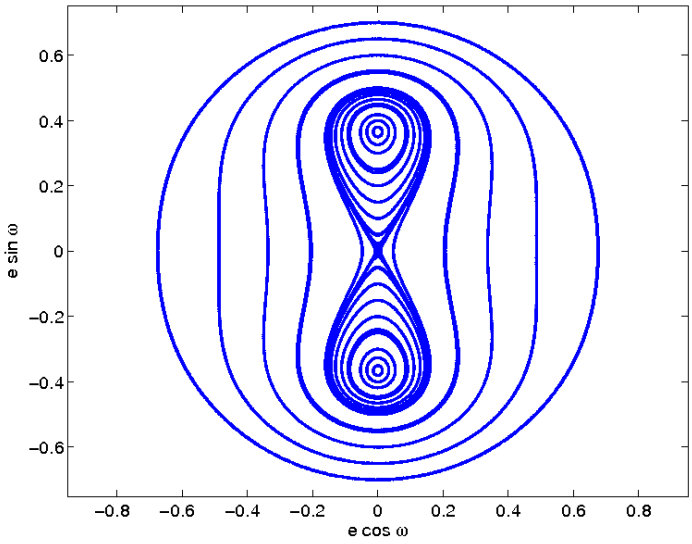

Figure 8. Restricted three-body problem phase space, corresponding to $H = 0.41833$, and reproducing the Kozai resonance (see the text for further details). Initial conditions for the calculation are the following: $a = 0.35$, $a_{giant} = 1$, $e_{giant} = 0$, $i_{giant} = 0$ where the subscript *giant* refers to the outer giant planet.

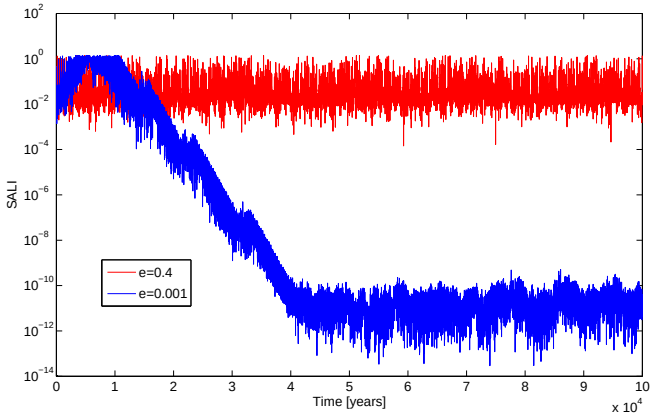

Figure 9. `SALI` characterization of two orbits of Figure 8 with a symplectic $SABA_{10}$ scheme: a regular orbit at $e = 0.4$ (red) and a chaotic orbit at $e = 0.001$ (blue).

shown in Figure 10. The chaos along the separatrix is clearly visible for values of $e \sin \omega$ close to 0 and to 0.5.

In order to compare our method with a non-symplectic scheme, we tried to reproduce these results with the Bulirsch-Stoer integration method. The first comment is that this adaptive stepsize method requires computation times up to three times longer than the global symplectic integrator. Secondly, it appears that this non-symplectic method seems unable to characterize correctly the orbits, regardless of the time step

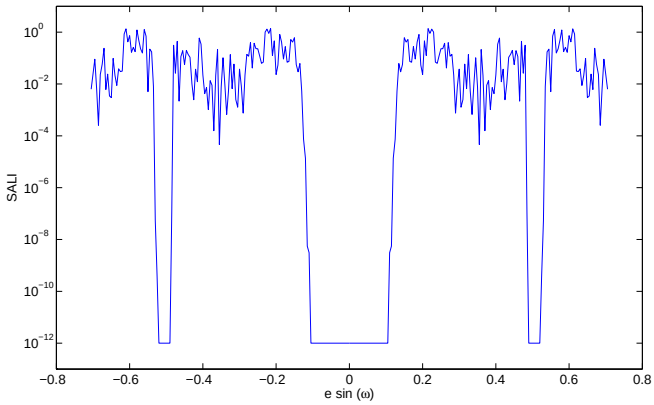

Figure 10. `SALI` characterization of the global behavior of Figure 8 as a function of $e \sin \omega$, after $100,000$ years. In order to avoid useless computation time, `SALI` values have been fixed to 10^{-12} when reaching this threshold. The influence of the separatrix is obvious and well identified by our symplectic $SABA_{10}$ scheme.

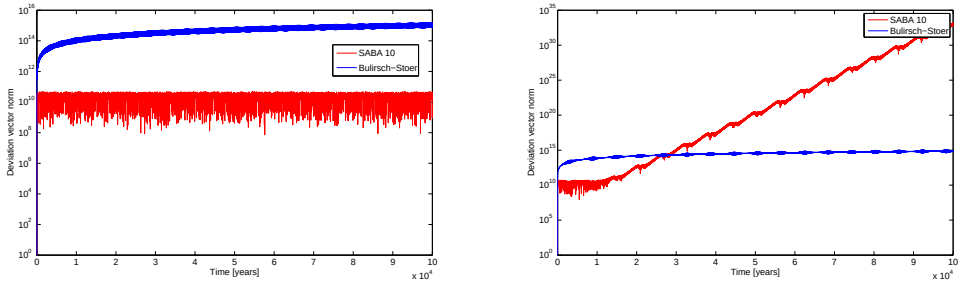

Figure 11. Norm of the deviation vector computed with $SABA_{10}$ symplectic scheme (red curves) and Bulirsch-Stoer method (blue curves) for the two orbits of Figure 9.

used. Indeed, even if the orbit is correctly described by the Bulirsch-Stoer method, the deviation vectors do not enable us to distinguish a regular behavior from a chaotic one. To show this, we reported in Figure 11 the norm of the same deviation vector integrated with our symplectic scheme (red curves) and with the Bulirsch-Stoer method (blue curves). Using the $SABA_{10}$ method, the norm of the deviation vector grows very rapidly for the chaotic orbit identified in Figure 9. On the contrary, no significant deviation is observed between the two orbits of Figure 9 for the non-symplectic method. Maybe, the integration on a longer time span with the Bulirsch-Stoer method would eventually reveal the chaotic behavior of one of these two orbits. Anyway, given that the energy is not fully conserved, one could not reliably trust this result, even more on long time interval.

5. Conclusions

In this work, we proposed a new method for the detection of regular and chaotic orbits in Hamiltonian systems, based on the integration of the deviation vectors used in chaos detection techniques, using symplectic algorithms. Our method has been tested on two well-known models, and the results clearly demonstrate that it outperforms non-symplectic ones.

Concerning the Hénon-Heiles system, it appears that, for large time steps, non-symplectic integrators tend to detect an excessive number of chaotic orbits, while the global symplectic integrator is able to identify correctly the character of nearly all orbits for larger time steps, up to four times larger than non–symplectic ones. Moreover, due to his symplectic properties, we showed that our method ensures a very small energy loss even on very long time spans. Let us emphasize that the possibility to use larger time steps saves a considerable amount of computation time.

This possibility turns out to be essential for the study of the Kozai resonance in the restricted three-body problem, where the secular orbital changes operate on extremely long time scales. Once again, the influence of the separatrix of this problem is well identified by our global symplectic integrator. On the contrary, the Bulirsch-Stoer non-symplectic method, even with smaller time steps, seems unable to distinguish between regular and chaotic motion, at least on the same integration time span. A possible reason for this behavior could be the accumulation of numerical errors introduced by the integrator and a significant energy loss, disadvantages which are avoided using our symplectic scheme.

We are confident that our findings should be generic for a large class of Hamiltonian systems. Thus we encourage scientists working on chaos indicators to perform symplectic integrations of both the orbit and the deviation vectors using the global symplectic integrator, as proposed in the present paper, whenever the Hamiltonian is of the form $H(\vec{x}) = A(\vec{p}) + B(\vec{q})$, or generically it can be divided into two parts, each one separately integrable. Computation time and reliability of the results could thus benefit a lot from this procedure, as we clearly demonstrated above.

Acknowledgments

The work of A.-S. L. is supported by an FNRS Postdoctoral Research Fellowship. The work of Ch. H. is supported by an FNRS PhD Fellowship. Numerical simulations were made on the local computing resources (Cluster URBM-SYSDYN) at the University of Namur (FUNDP, Belgium). The authors want to thank Ch. Antonopoulos for his constructive suggestions that we used to improve a previous version of our work.

References

[1] C. Froeschlé, E. Lega and R. Gonczi, Fast Lyapunov indicators. Application to asteroidal motion, Celest. Mech. and Dyn. Astr. 67 (1997) 41–62.

[2] P.M. Cincotta and C. Simó, Simple tools to study global dynamics in non-axisymmetric galactic potentials - I, Astronomy and Astrophysics Supplement 147 (2000) 205–228.

[3] Ch. Skokos, Alignment indices: A new, simple method for determining the ordered or chaotic nature of orbits, J. Phys. A 34 (2001) 10029-10043.

[4] Ch. Skokos, T. Bountis and Ch. Antonopoulos, Geometrical properties of local dynamics in Hamiltonian systems: The Generalized Alignment Index (GALI) method, Physica D 231 (2007) p 30–54.

[5] J. Laskar, C.Froeschlé and A.Celletti, The measure of chaos by the numerical analysis of the fundamental frequencies. Applications to the standard mapping, Physica D 56 (1992) 253–269.

[6] J.Laskar, Frequency analysis for multi-dimensional systems. Global dynamics and diffusion, Physica D 67 (1993) 257–281.

[7] M. Guzzo and G. Benettin, A spectral formulation of the Nekhoroshev theorem and its relevance for numerical and experimental data anlysis, Discrete and Continous Dynamical Systems-Series B 1 (2001) 1–28.

[8] J. Laskar and Ph. Robutel, High order symplectic integrators for perturbed hamiltonian systems, Cel. Mec. 80 (2001) 39–62.

[9] N. Bourbaki, Eléments de Mathématiques: Groupes et Algèbres de Lie, Hermann Ed. Paris, (1972).

[10] Ch. Skokos, Ch. Antonopoulos, T. C. Bountis and M. N. Vrahatis, How Does the Smaller Alignment Index (SALI) Distinguish Order from Chaos?, Prog. Theor. Phys. Supp. 150 (2003) 439–443.

[11] A. Széll, B. Érdi, Zs. Sándor and B. Steves, Chaotic and stable behaviour in the Caledonian Symmetric Four-Body Problem, MNRAS 347 (2004) 380–388.

[12] T. Manos and E. Athanassoula E, Detecting chaotic and ordered motion in barred galaxies, Proceedings of Semaine de l' Astrophysique Française Journées de la SF2A, eds F Caloli, T Contini, J M Hameury and L Pagani (EDP-Science Conference Series), 2005, pp. 631.

[13] J. Boreux et al., Improve beam stability in particle accelerators by using Hamiltonian control, preprint (2010).

[14] Ch. Skokos, Ch. Antonopoulos, T. C. Bountis and M. N. Vrahatis, Detecting order and chaos in Hamiltonian systems by the SALI method, J. Phys. A 37 (2004) 6269–6284.

[15] G. Benettin, L. Galgani, A. Giorgilli, J.-M. Strelcyn, Lyapunov characteristic exponents for smooth dynamical systems and for Hamiltonian systems; a method for computing all of them. Part 1: Theory, Meccanica 15 (1980) 9–20.

[16] Ch. Skokos, T. C. Bountis and Ch. Antonopoulos, Detecting chaos, determining the dimensions of tori and predicting slow diffusion in Fermi-Pasta-Ulam lattices by the Generalized Alignment Index method, Eur. Phys. J. Sp. T. 165 (2008) 5–14.

[17] M. Hénon and C. Heiles, The applicability of the third integral of motion: Some numerical experiments, Astron. J. 69 (1964) pp. 73-79.

[18] Y. Kozai, Secular perturbations of asteroids with high inclination and eccentricity, AJ 67 (1962) 591–598

[19] A.-S. Libert and K. Tsiganis, Kozai resonance in extrasolar system, A&A 493 (2009) 677-686

[20] F. Malige, P. Robutel, J. Laskar, Partial Reduction in the N-Body Planetary Problem using the Angular Momentum Integral, Celest. Mech. & Dyn. Astro. 84 (2002), 283–316

[21] F. Thomas and A. Morbidelli, The Kozai Resonance in the Outer Solar System and the Dynamics of Long-Period Comets, Celest. Mech. & Dyn. Astro. 64 (1996) 209–299

[22] B. Funk, A.-S. Libert, A. Suli, E. Pilat-Lohinger, On the influence of the Kozai resonance in habitable zones of extrasolar planetary systems, preprint (2010)

[23] M. J. Duncan, H. F. Levison, M. H. Lee, A Multiple Time Step Symplectic Algorithm for Integrating Close Encounters, AJ 116 (1998) 2067–2077